第 44 卷 第 7 期/2024 年 4 月/光学学报 研究论文

光学学报

# 基于速度比的光楔扫描轨迹选取方法

段霖森[1]，谢洪波[1]，马骏[2*]，杨磊[1]

[1]天津大学精密仪器与光电子工程学院光电信息技术教育部重点实验室，天津 300072；

[2]西安工业大学兵器科学与技术学院，陕西 西安 710021

**摘要** 基于非近轴光线追迹算法对光楔扫描系统的正向问题进行求解，得到不同速度比下的花瓣形扫描轨迹。根据光楔转速和取样间隔计算轨迹点数，根据轨迹点与坐标原点的距离曲线的极小值点个数计算花瓣数，进而建立由速度比计算花瓣数的关系式。通过轨迹点数和花瓣数评估不同速度比对应的扫描轨迹的扫描时间和覆盖率，总结扫描轨迹与速度比之间的规律，提出三光楔扫描系统获取规则、对称且不存在大片扫描盲区的扫描轨迹时速度比需要满足的条件。所得规律和结论可在光楔扫描系统的应用中合理确定速度比，从而选取满足扫描效率要求的扫描轨迹。

**关键词** 光学设计；光楔；非近轴光线追迹；花瓣形扫描轨迹；速度比

**中图分类号** O436 **文献标志码** A **DOI**：10.3788/AOS231834

## 1 引 言

常见的扫描系统主要采用万向框架式和反射镜式结构[1-2]，这两种结构都需要机械伺服转台协助实现光束扫描和指向，且具有系统体积大、质量重、功耗大、灵敏度低等缺点[3-4]。光楔扫描系统为传统扫描方式提供了有益补充，相比之下，其具有结构紧凑、扫描视场大、指向精度高、动态性能好、光损耗小、对载体振动不敏感等优点[5]，是设计轻小型化激光扫描系统的理想选择之一。

光楔扫描系统多采用双光楔，相应的技术成熟度较高，能满足多数情况下的扫描和指向需求。然而，双光楔扫描系统也存在固有扫描盲区和“过顶问题”，这些缺陷可以通过三光楔扫描系统来消除[6-7]，但是三光楔的控制更复杂，目前并没有得到广泛研究和应用。总的来说，关于光楔扫描系统的研究主要集中在光楔的正反向问题、光束扫描模式、“过顶问题”、光楔引起的光束变形和成像畸变、扫描性能和指向精度的影响因素、光楔旋转控制等方面[8]，基于这些研究，国内外也在激光雷达、激光通信和激光制导等领域应用光楔扫描系统并取得了一些成果[9-13]。

实际应用中，合理选取扫描轨迹是十分重要的，这会直接影响系统的扫描效率。在光楔参数和相对位置确定的情况下，光楔旋转速度比是可变且可控的，从而可以得到不同形状的扫描轨迹。目前，此类研究主要集中在扫描轨迹的具体实现，例如：Marshall[14]基于近轴矢量算法研究了双光楔的扫描模式，分析了不同楔角、不同转速、不同初始方位角下的扫描图案；Dimb等[15]将与光楔扫描轨迹相关的参数输入到机械设计程序CATIA V5R20中，通过程序自动确定各参数以实现目标扫描轨迹选取。由于对扫描轨迹与速度比内在规律的研究较少，通过速度比选取合理的扫描轨迹仍缺乏相关依据。

本文基于非近轴光线追迹算法对光楔扫描系统的正向问题进行求解，得到不同速度比下的扫描轨迹，并分析二者之间的规律。通过建立速度比与扫描轨迹点数和花瓣数之间的关系，评估不同速度比下扫描轨迹的扫描时间与覆盖率，从而在光楔扫描系统的实际应用中通过合理确定速度比来选取满足扫描效率要求的扫描轨迹。

## 2 基本原理

光楔扫描系统通过控制光楔的共轴旋转来改变出射光束的偏转状态，从而进行光束扫描和指向[16]。光楔扫描系统的正向问题是指已知光楔各自独立的旋转角度，求解此时出射光束的指向方位，随着光楔旋转角度的连续变化，则可得到系统的扫描轨迹。目前，关于双光楔正向问题的求解已经得到了广泛的研究，常用的求解方法有近轴矢量算法[17-20]、旋转矩阵算法[21-22]和非近轴光线追迹算法[23-26]。其中，非近轴光线追迹算法可推导出正向问题的准确解析解，适用于任意楔角大小的光楔，且该方法也可由双光楔轻易扩展到三光

**收稿日期**：2023-11-24；**修回日期**：2024-01-15；**录用日期**：2024-01-22；**网络首发日期**：2024-02-20

**通信作者**：*majun@xatu.edu.cn

楔或更多光楔的扫描系统。

光线追迹算法是在三维空间坐标系中，将入射光束看作空间直线，光楔表面看作空间平面，并将这些直线和平面的立体几何基本要素用矩阵表示，将几何运算转化为矩阵运算。根据空间矢量形式的折射定律，从入射光束开始，逐面计算折射光束的走向，最终得到出射光束的指向方位。空间直线和平面可分别用矩阵表示为

$$\boldsymbol{l}=\begin{bmatrix} x_0 & a \\ y_0 & b \\ z_0 & c \end{bmatrix},\ \boldsymbol{F}=\begin{bmatrix} A \\ B \\ C \\ D \end{bmatrix}, \tag{1}$$

式中：$(x_0, y_0, z_0)$为直线$\boldsymbol{l}$经过的一点；$(a, b, c)$为直线$\boldsymbol{l}$的方向向量；$(A, B, C)$为平面$\boldsymbol{F}$的法向量。此时直线$\boldsymbol{l}$与平面$\boldsymbol{F}$的交点为

$$\boldsymbol{P}=\begin{bmatrix} x_0 \\ y_0 \\ z_0 \end{bmatrix}-k\begin{bmatrix} a \\ b \\ c \end{bmatrix}, \tag{2}$$

式中：$k=\dfrac{D+(A,B,C)(x_0,y_0,z_0)}{(A,B,C)(a,b,c)}$。

设入射和折射光线的方向矢量分别为$\boldsymbol{A}_{\text{in}}$、$\boldsymbol{A}_{\text{out}}$，折射率分别为$n_{\text{in}}$、$n_{\text{out}}$，折射表面的单位法向量为$\boldsymbol{N}$，则矢量形式的折射定律可以表示为

$$\boldsymbol{A}_{\text{out}}=\frac{n_{\text{in}}}{n_{\text{out}}}\left[\boldsymbol{A}_{\text{in}}-(\boldsymbol{N}\cdot\boldsymbol{A}_{\text{in}})\boldsymbol{N}\right]+\boldsymbol{N}\sqrt{1-\left(\frac{n_{\text{in}}}{n_{\text{out}}}\right)^2\left[1-(\boldsymbol{N}\cdot\boldsymbol{A}_{\text{in}})^2\right]}。 \tag{3}$$

对式(3)进行变形[27]，可得到

$$\boldsymbol{A}_{\text{out}}=\boldsymbol{A}_{\text{in}}+\Gamma\boldsymbol{N}, \tag{4}$$

式中：$\Gamma=\sqrt{n_{\text{out}}^2-n_{\text{in}}^2+(\boldsymbol{N}\cdot\boldsymbol{A}_{\text{in}})^2}-\boldsymbol{N}\cdot\boldsymbol{A}_{\text{in}}$。

以双光楔扫描系统为例，光楔排列方式及坐标系建立如图1所示：以光楔1后表面中心为原点建立空间直角坐标系，光楔楔角均为$\beta$，中心厚度均为$d$，双光楔间距为$d_1$，光楔2与目标平面$\boldsymbol{F}_5$的间距为$L$，双光楔分别以速度$\omega_1$、$\omega_2$旋转。图1中的入射光线$\boldsymbol{A}$、光楔表面$\boldsymbol{F}_1$～$\boldsymbol{F}_4$及目标平面$\boldsymbol{F}_5$的矩阵表达式分别为

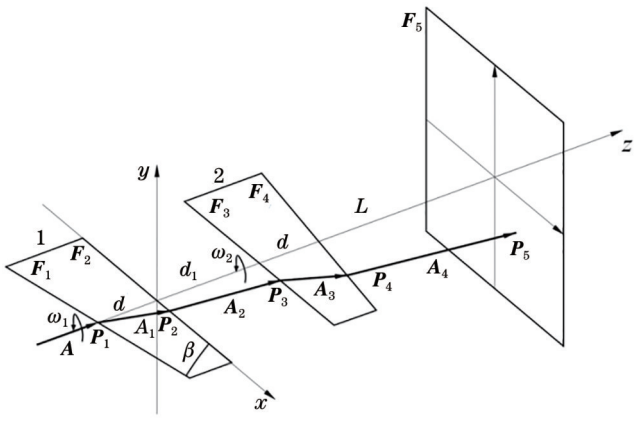


图1　双光楔排列方式及坐标系建立

Fig. 1　Arrangement of two-element Risley prisms and establishment of coordinate system

$$\boldsymbol{A}=\begin{bmatrix} 0 & 0 \\ 0 & 0 \\ 0 & 1 \end{bmatrix}, \tag{5}$$

$$\boldsymbol{F}_1=\begin{bmatrix} -\sin\beta\cos\theta_1 & -\sin\beta\sin\theta_1 & \cos\beta & d\cos\beta \end{bmatrix}^{\mathrm{T}}, \tag{6}$$

$$\boldsymbol{F}_2=\begin{bmatrix} 0 & 0 & 1 & 0 \end{bmatrix}^{\mathrm{T}}, \tag{7}$$

$$\boldsymbol{F}_3=\begin{bmatrix} 0 & 0 & 1 & -d_1 \end{bmatrix}^{\mathrm{T}}, \tag{8}$$

$$\boldsymbol{F}_4=\begin{bmatrix} \sin\beta\cos\theta_2 & \sin\beta\sin\theta_2 & \cos\beta & -(d+d_1)\cos\beta \end{bmatrix}^{\mathrm{T}}, \tag{9}$$

$$\boldsymbol{F}_5=\begin{bmatrix} 0 & 0 & 1 & -(d+d_1+L) \end{bmatrix}^{\mathrm{T}}, \tag{10}$$

式中：$\theta_1$和$\theta_2$分别为光楔1和光楔2的旋转角度。当光线$\boldsymbol{A}$入射到表面$\boldsymbol{F}_1$时，可分别通过式(2)和式(4)求得交点$\boldsymbol{P}_1$和光线$\boldsymbol{A}_1$的方向矢量$\boldsymbol{A}_{1\text{out}}$，即可得到光线$\boldsymbol{A}_1=[\boldsymbol{P}_1 \quad \boldsymbol{A}_{1\text{out}}]$。以此类推，可求出光线$\boldsymbol{A}_4$及其与目标平面的交点$\boldsymbol{P}_5$，从而得到出射光束的指向方位。对于三光楔扫描系统，其正向问题的求解方法与双光楔相同，只是多了两个光楔表面追迹。

## 3　轨迹点数与花瓣数的计算

所采用的光楔楔角为11.85°，材料为H-K9L，光楔1与光楔2的间距为3 mm，光楔2与光楔3的间距为5 mm。对于双光楔扫描系统，若光楔旋转速度的单位为(°)/s，以1 s为间隔取样，则光楔1和光楔2旋转一圈分别有$\left|360/\omega_1\right|$和$\left|360/\omega_2\right|$个轨迹点，当光楔1和光楔2同时从零位开始旋转，并第一次同时回到零位时，它们完成了一次全视场扫描，此时双光楔的扫描轨迹点数为$\left|360/\omega_1\right|$和$\left|360/\omega_2\right|$的最小公倍数，轨迹点数可评估全视场扫描所需的时间。如图2所示，当$\omega_1=3$(°)/s时，分别取$\omega_2=-4.5$(°)/s和$\omega_2=13.92$(°)/s，此时完成一次全视场扫描的轨迹点数分别为240和3000，对应的扫描时间分别为240 s和3000 s。

对于图2中的花瓣形扫描轨迹，依次求出每个轨迹点与原点的距离并绘制曲线，结果如图3所示。可见，每个花瓣的最低点与原点的距离为整个曲线的极小值点，即该扫描轨迹的花瓣数等于距离曲线的极小值点个数，则花瓣数分别为5和91。

对于三光楔扫描系统，完成一次全视场扫描时的轨迹点数为$\left|360/\omega_1\right|$、$\left|360/\omega_2\right|$和$\left|360/\omega_3\right|$的最小公倍数，其扫描轨迹花瓣数同样等于上述距离曲线的极小值点个数。

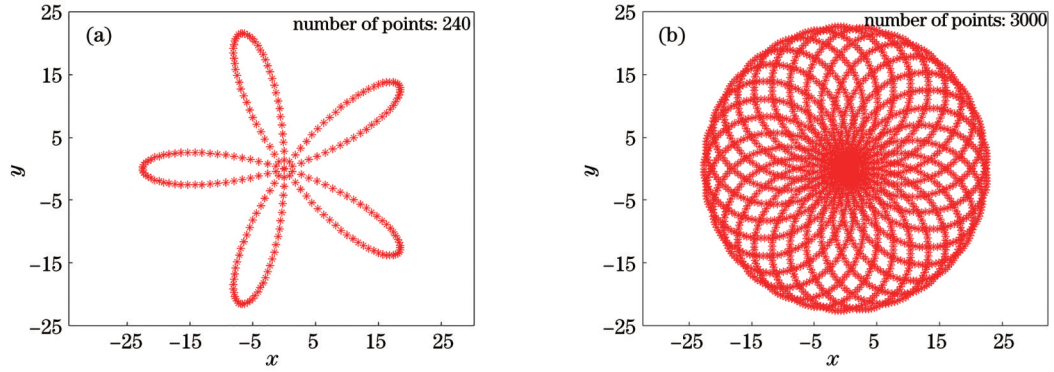


图 2　扫描轨迹点数。(a) $\omega_1=3(^\circ)/s,\omega_2=-4.5(^\circ)/s$;(b) $\omega_1=3(^\circ)/s,\omega_2=13.92(^\circ)/s$

Fig. 2　Number of points of scanning trajectories. (a) $\omega_1=3(^\circ)/s,\omega_2=-4.5(^\circ)/s$; (b) $\omega_1=3(^\circ)/s,\omega_2=13.92(^\circ)/s$

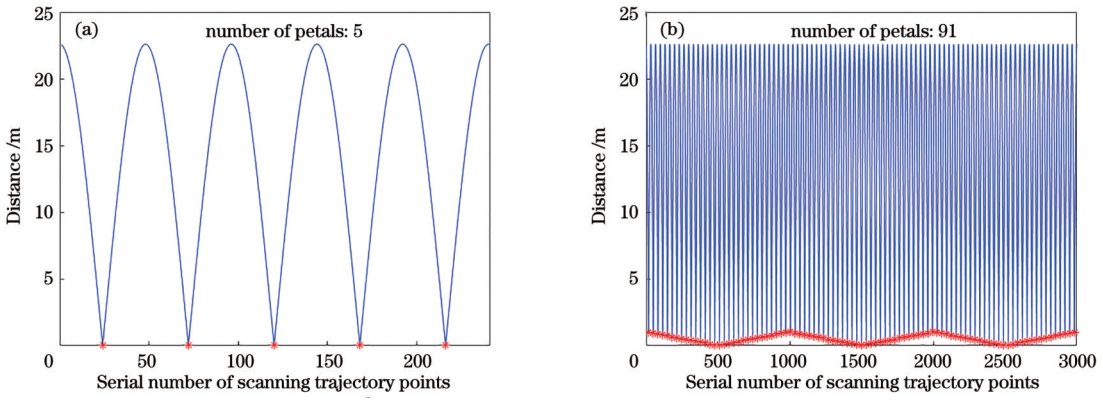


图 3　扫描轨迹花瓣数。(a) $\omega_1=3(^\circ)/s,\omega_2=-4.5(^\circ)/s$;(b) $\omega_1=3(^\circ)/s,\omega_2=13.92(^\circ)/s$

Fig. 3　Number of petals of scanning trajectories. (a) $\omega_1=3(^\circ)/s,\omega_2=-4.5(^\circ)/s$; (b) $\omega_1=3(^\circ)/s,\omega_2=13.92(^\circ)/s$

## 4　扫描轨迹与速度比之间的规律

### 4.1　双光楔扫描系统

对于双光楔扫描系统，设光楔的旋转速度比为 $M=\omega_2/\omega_1$，$M$ 的小数部分用 $m$ 表示，小数位数用 $n$ 表示（考虑到电机转速控制精度，令 $n\leqslant 2$），轨迹点数用 $N_g$ 表示，花瓣数用 $N_h$ 表示。经过分析，可以得到双光楔扫描轨迹的几点规律：

1）通过求解距离曲线的极小值点个数获取扫描轨迹花瓣数，进而分析和总结花瓣数与速度比之间的数值规律，发现双光楔扫描轨迹花瓣数与速度比之间存在如下关系：

$$N_h=|M-1|\times 10^n/t。\tag{11}$$

当 $M$ 为整数时，$t=1$。当 $M$ 为小数时：若 $m\times 10^n$ 为奇数，则 $m\times 10^n$ 为 5 的倍数时 $t=5$，$m\times 10^n$ 为 25 的倍数时 $t=25$，其余情况下 $t=1$；若 $m\times 10^n$ 为偶数，则 $n=2$ 且 $m\times 10^n$ 为 4 的倍数时 $t=4$，其余情况下 $t=2$。根据分类选取不同的速度比，其扫描轨迹如表 1 和图 4 所示。

从表 1 和图 4 可以看出（假设 $\omega_1$ 固定）：$M$ 为正数

表 1　$\omega_1=1(^\circ)/s$ 时不同速度比下的轨迹点数与花瓣数

Table 1　Number of points and petals of scanning trajectories with $\omega_1=1(^\circ)/s$ at different velocity ratios

| Condition | $M$ | $N_g$ | $N_h$ |
|---|---|---|---|
| $M$ is an integer | 3 | 360 | 2 |
| | −4 | 360 | 5 |
| | 5 | 360 | 4 |
| | −6 | 360 | 7 |
| $M$ is a decimal, $m\times 10^n$ is a multiple of 5 | 2.5 | 720 | 3 |
| | −2.15 | 7200 | 63 |
| | 0.45 | 7200 | 11 |
| | −3.35 | 7200 | 87 |

续表

| Condition | $M$ | $N_g$ | $N_h$ |
|---|---|---|---|
| $M$ is a decimal, $m \times 10^n$ is a multiple of 25 | 1.25 | 1440 | 1 |
| | −1.75 | 1440 | 11 |
| | 3.25 | 1440 | 9 |
| | −4.75 | 1440 | 23 |
| $M$ is a decimal, $m \times 10^n$ is the rest of the odd numbers | 0.9 | 3600 | 1 |
| | −1.03 | 36000 | 203 |
| | 1.3 | 3600 | 3 |
| | −1.17 | 36000 | 217 |
| $M$ is a decimal, $n=2$ and $m \times 10^n$ is a multiple of 4 | 1.04 | 9000 | 1 |
| | −2.24 | 9000 | 81 |
| | 2.48 | 9000 | 37 |
| | −3.36 | 9000 | 109 |
| $M$ is a decimal, $m \times 10^n$ is the rest of the even numbers | 2.2 | 1800 | 6 |
| | −1.06 | 18000 | 103 |
| | 2.8 | 1800 | 9 |
| | −2.02 | 18000 | 151 |

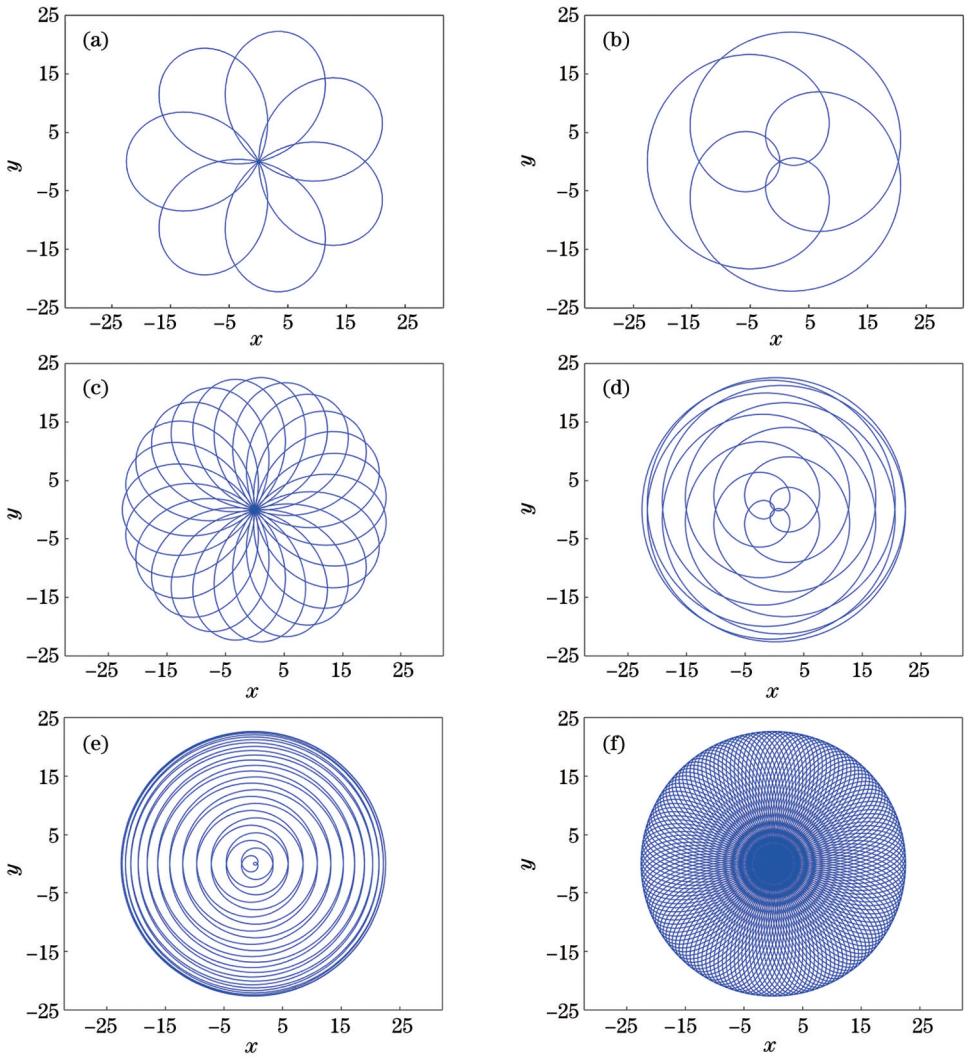


图 4 不同速度比下的扫描轨迹。(a) $M=-6$;(b) $M=2.5$;(c) $M=-4.75$;(d) $M=1.3$;(e) $M=1.04$;(f) $M=-2.02$

Fig. 4 Scanning trajectories at different velocity ratios. (a) $M=-6$; (b) $M=2.5$; (c) $M=-4.75$; (d) $M=1.3$; (e) $M=1.04$; (f) $M=-2.02$

时，扫描轨迹为内花瓣；$M$为负数时，扫描轨迹为外花瓣。$M$为整数时，不同速度比的轨迹点数相同，即完成一次全视场扫描的时间相同。$M$为小数时，在每一类中：当$n$相同时，不同速度比下的轨迹点数分别相同，即扫描时间相同；当$n$不同时，则$n$越大，轨迹点数越多，即扫描时间越长，而且呈10的倍数增长。因此，为了避免扫描时间过长，速度比的小数位数不宜过多。在每一类中，$M$同号时，$|M|$越大，则花瓣数越多，扫描轨迹覆盖率越大。

2）取不同速度比时可能得到相同花瓣数，但此时扫描轨迹也不同，如表2和图5所示。若$M$同号，当$n$相同时，$|M|$越小，则轨迹点数越多，扫描时间越长，扫描轨迹覆盖率越大；当$n$不同时，$n$越大，则轨迹点数越多，扫描时间越长，扫描轨迹覆盖率越大。

3）由于双光楔具有对称性，当$|M|<1$时，可以转换成$|M|>1$的整数或小数。如表3和图6所示：$M$=0.2=1∶5可以等效为$M$=5=5∶1，即$M$=0.2和$M$=5

表2　$\omega_1=1(°)/s$时不同速度比下的轨迹点数与花瓣数

Table 2　Number of points and petals of scanning trajectories with $\omega_1=1(°)/s$ at different velocity ratios

| $M$ is positive | | | $M$ is negative | | |
|---|---|---|---|---|---|
| $M$ | $N_g$ | $N_h$ | $M$ | $N_g$ | $N_h$ |
| 1.7 | 3600 | 7 | −4.7 | 3600 | 57 |
| 4.5 | 720 | 7 | −27.5 | 720 | 57 |
| 1.14 | 18000 | 7 | −1.28 | 9000 | 57 |
| 2.4 | 1800 | 7 | −10.4 | 1800 | 57 |
| 1.07 | 36000 | 7 | −0.14 | 18000 | 57 |
| 1.35 | 7200 | 7 | −1.85 | 7200 | 57 |

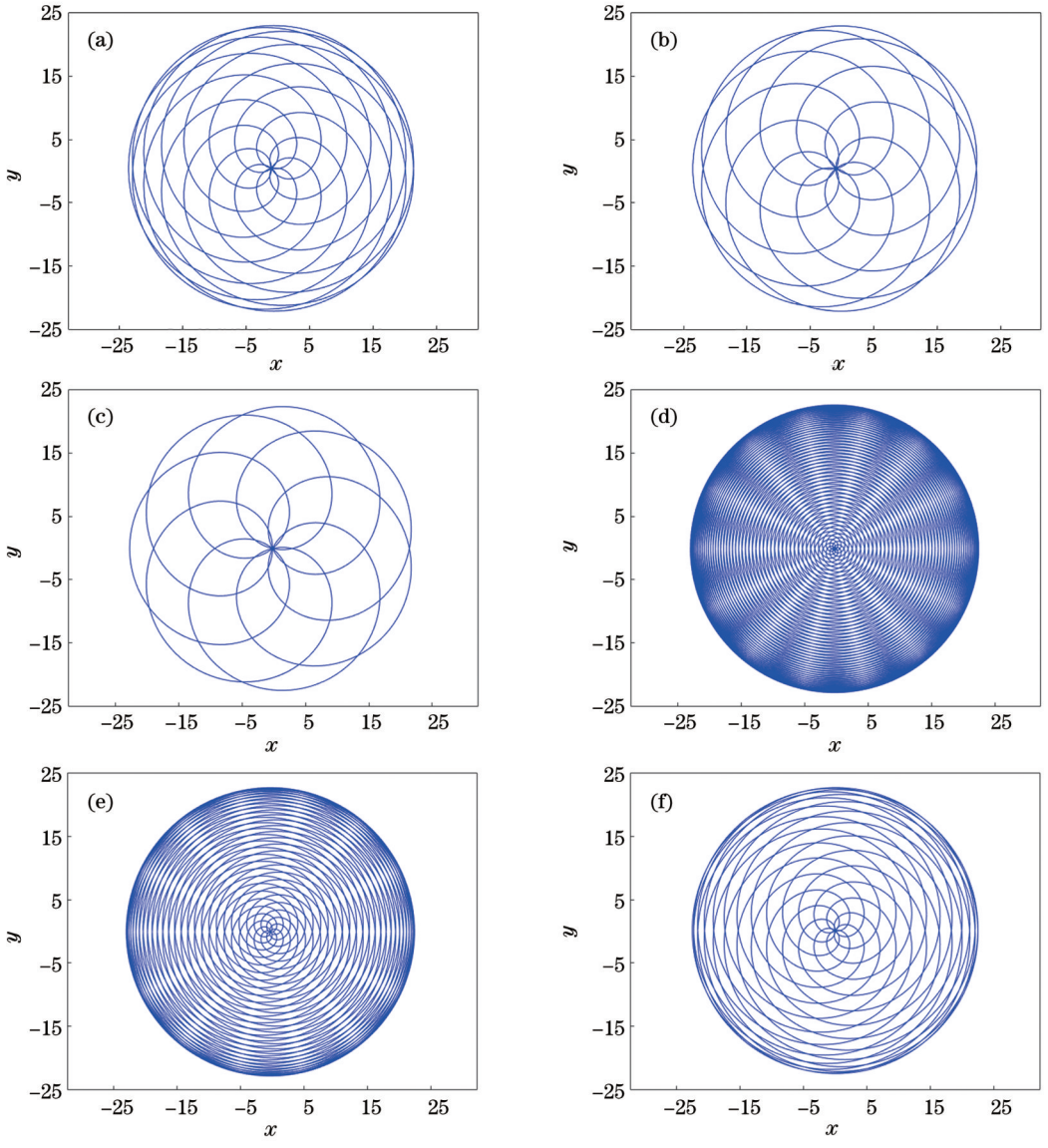


图5　相同花瓣数下的扫描轨迹。(a) $M$=1.7；(b) $M$=2.4；(c) $M$=4.5；(d) $M$=1.07；(e) $M$=1.14；(f) $M$=1.35

Fig. 5　Scanning trajectories with the same number of petals. (a) $M$=1.7; (b) $M$=2.4; (c) $M$=4.5; (d) $M$=1.07; (e) $M$=1.14; (f) $M$=1.35

表 3　$\omega_1=1(°)/s$时不同速度比下的轨迹点数与花瓣数

Table 3　Number of points and petals of scanning trajectories with $\omega_1=1(°)/s$ at different velocity ratios

| $M$ | $N_g$ | $N_h$ | $M$ | $N_g$ | $N_h$ |
|---|---|---|---|---|---|
| 0.25 | 1440 | 3 | 4 | 360 | 3 |
| −0.4 | 1800 | 7 | −2.5 | 720 | 7 |

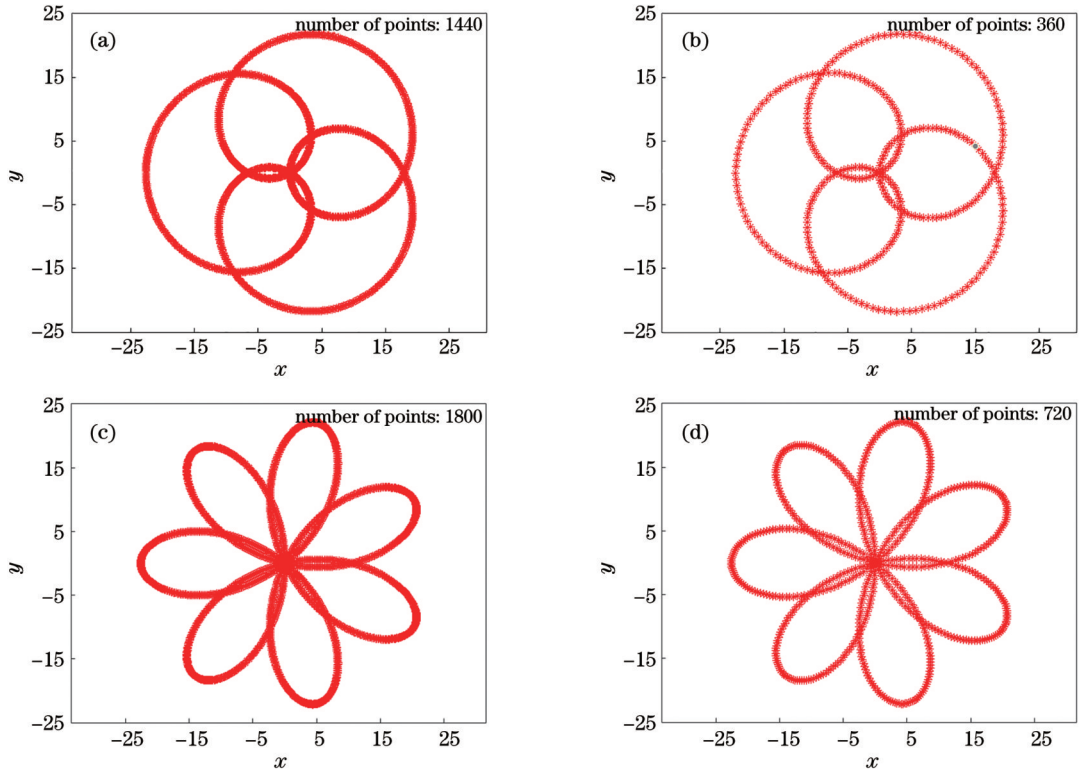


图 6　相同形状下的扫描轨迹点。(a) $M$=0.25; (b) $M$=4; (c) $M$=−0.4; (d) $M$=−2.5

Fig. 6　Points of scanning trajectories in the same shape. (a) $M$=0.25; (b) $M$=4; (c) $M$=−0.4; (d) $M$=−2.5

时的扫描轨迹形状相同，其覆盖率相同，但二者轨迹点数不同，这是因为光楔 1 的转速 $\omega_1$ 固定且以其为基准，$M=0.2$ 时双光楔的转速更慢，因此轨迹点数更多，扫描时间更长。

### 4.2　三光楔扫描系统

对于三光楔扫描系统，设光楔旋转速度比为 $M_1=\omega_2/\omega_1$、$M_2=\omega_3/\omega_1$，基于对双光楔扫描轨迹的分析，可以得到三光楔扫描轨迹的几点规律：

1) 在 $M_1=M_2$ 条件下，三光楔扫描轨迹与速度比为 $M_1$(或 $M_2$)时的双光楔扫描轨迹形状相同，但由于光楔对光束的偏转相互抵消，其中心会有一个圆形扫描盲区，如图 7 所示。

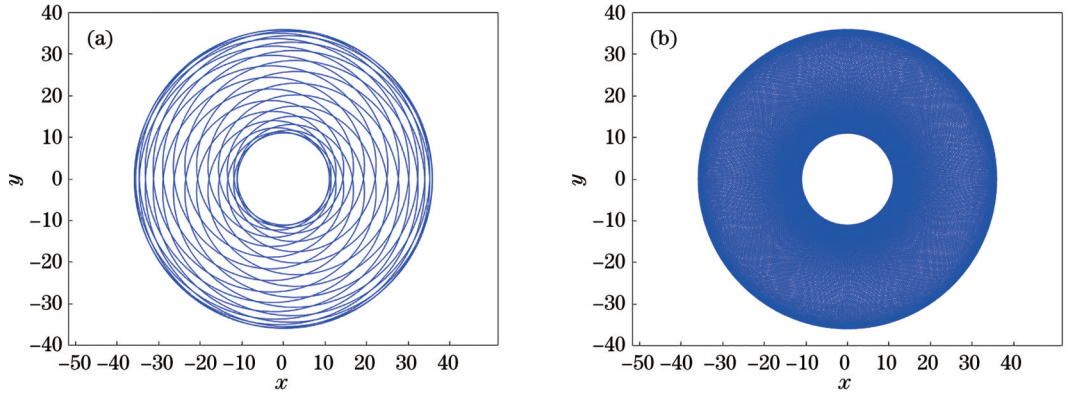


图 7　$M_1=M_2$时的扫描轨迹。(a) $M_1=M_2=1.35$; (b) $M_1=M_2=-4.06$

Fig. 7　Scanning trajectories when $M_1=M_2$. (a) $M_1=M_2=1.35$; (b) $M_1=M_2=-4.06$

2）当$M_1=-M_2$时，三光楔扫描轨迹形状整体呈“条形”，在全视场扫描范围内存在大片扫描盲区，如图8所示。

3）当$|M_1|\neq|M_2|$时，若随机取$M_1$和$M_2$，则三光楔扫描轨迹很可能不规则或者存在较多的扫描盲区，如图9所示。

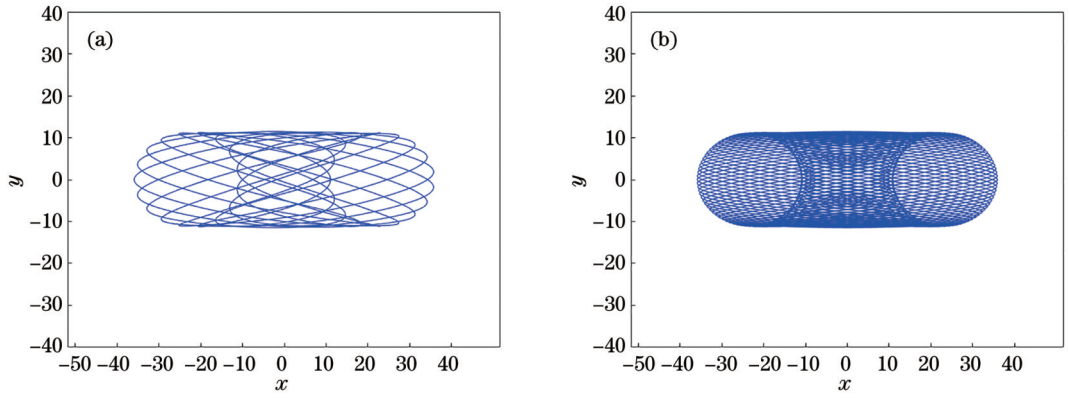


图8　$M_1=-M_2$时的扫描轨迹。(a) $M_1=-M_2=1.7$；(b) $M_1=-M_2=3.24$

Fig. 8　Scanning trajectories when $M_1=-M_2$. (a) $M_1=-M_2=1.7$; (b) $M_1=-M_2=3.24$

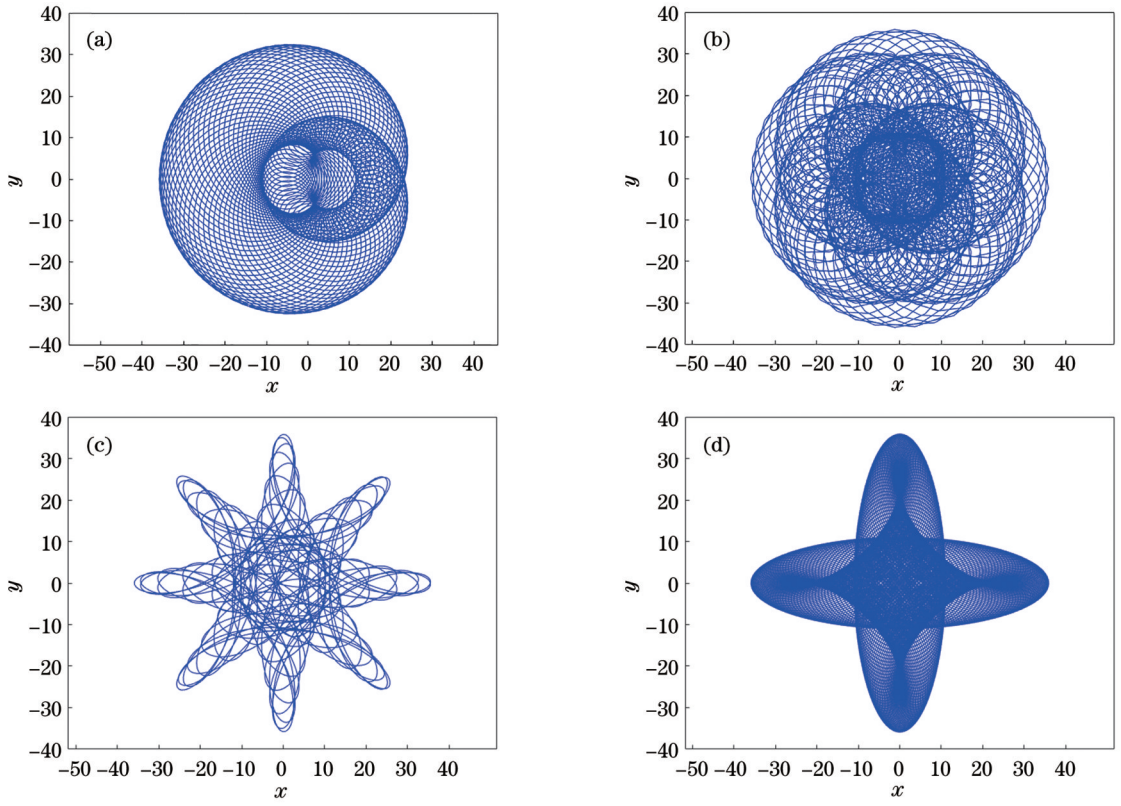


图9　$|M_1|\neq|M_2|$时的随机扫描轨迹。(a) $M_1=6.3$，$M_2=12.6$；(b) $M_1=-6.3$，$M_2=-24.9$；(c) $M_1=2.8$，$M_2=-5.7$；(d) $M_1=2.18$，$M_2=-5.36$

Fig. 9　Random scanning trajectories when $|M_1|\neq|M_2|$. (a) $M_1=6.3$, $M_2=12.6$; (b) $M_1=-6.3$, $M_2=-24.9$; (c) $M_1=2.8$, $M_2=-5.7$; (d) $M_1=2.18$, $M_2=-5.36$

若速度比分别取$M_1$和$M_2$时，对应的双光楔扫描轨迹花瓣数（分别用$N_{h1}$和$N_{h2}$表示）呈倍数（1～2倍）关系，其轨迹点数（分别用$N_{g1}$和$N_{g2}$表示）也呈倍数（1～2倍）关系，此时三光楔扫描轨迹是规则、对称且不存在大片扫描盲区的花瓣形轨迹，如表4和图10所示。

由表4和图10可见：当$M_1$和$M_2$同正时，扫描轨迹为内花瓣；当$M_1$和$M_2$同负或异号时，扫描轨迹为外花瓣。总的轨迹点数为$N_g=\max(N_{g1},N_{g2})$，总的花瓣数为$N_h=2\min(N_{h1},N_{h2})$。由于三光楔扫描轨迹的轨迹点数和花瓣数可以分别由$N_{h1}$和$N_{h2}$、$N_{g1}$和$N_{g2}$计算，故其扫描时间和覆盖率可沿用双光楔扫描轨迹的规律进行评估，此处不再赘述。

表 4 $\omega_1=1(°)/s$时不同速度比下的轨迹点数与花瓣数

Table 4 Number of points and petals of scanning trajectories with $\omega_1=1(°)/s$ at different velocity ratios

| Condition | $M_1$ | $N_{g1}$ | $N_{h1}$ | $M_2$ | $N_{g2}$ | $N_{h2}$ | $N_g$ | $N_h$ |
|---|---|---|---|---|---|---|---|---|
| $M_1$ and $M_2$ are both positive | 6.4 | 1800 | 27 | 11.8 | 1800 | 54 | 1800 | 54 |
| | 5.04 | 9000 | 101 | 9.08 | 9000 | 202 | 9000 | 202 |
| $M_1$ and $M_2$ are both negative | −3.5 | 720 | 9 | −1.25 | 1440 | 9 | 1440 | 18 |
| | −3.04 | 9000 | 101 | −7.08 | 9000 | 202 | 9000 | 202 |
| One of $M_1$ and $M_2$ is positive, and the other is negative | 8.1 | 3600 | 71 | −6.1 | 3600 | 71 | 3600 | 142 |
| | 6.02 | 18000 | 251 | −4.02 | 251 | 18000 | 18000 | 502 |

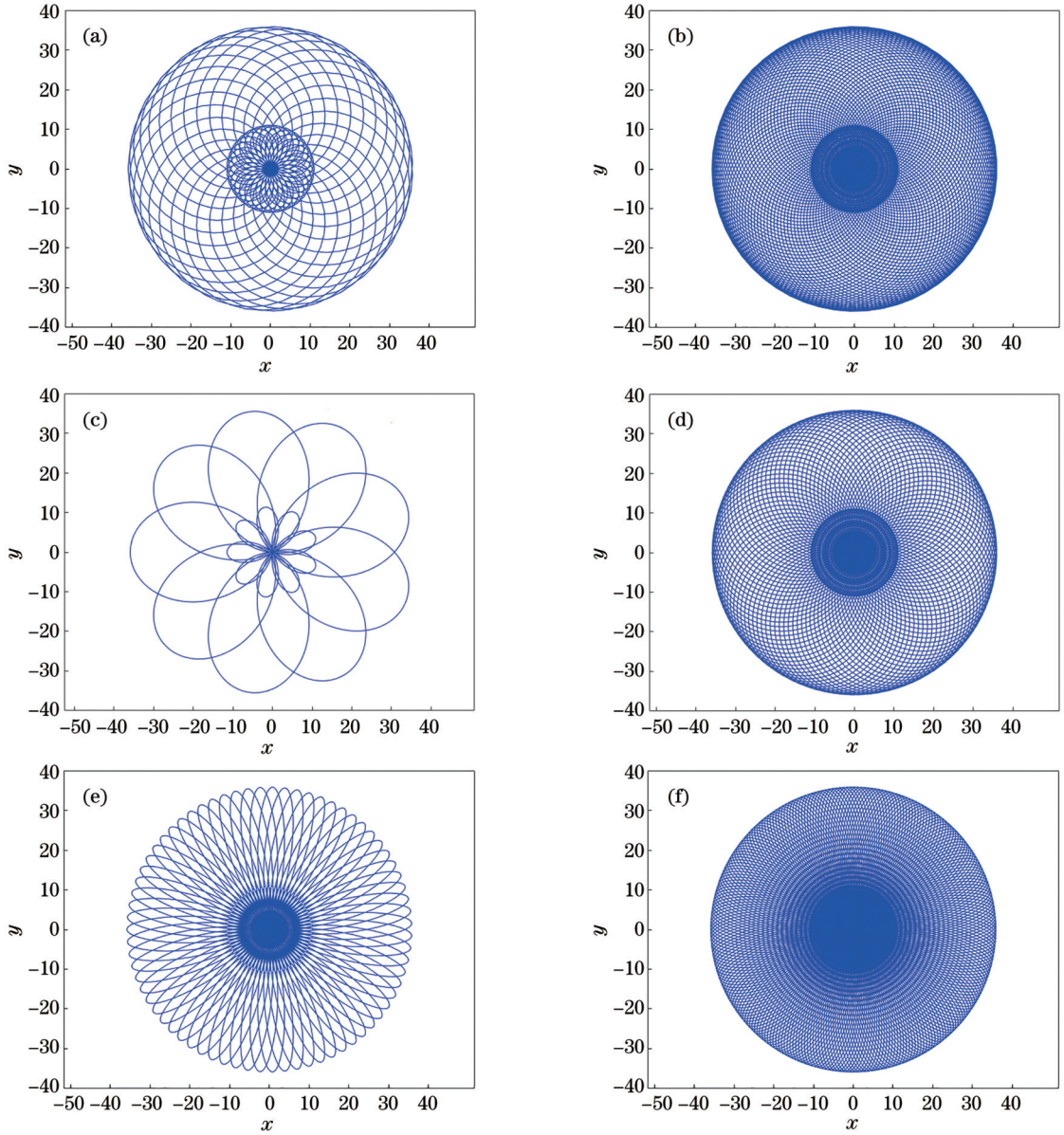


图 10 $|M_1|\neq|M_2|$时规则且对称的扫描轨迹。(a) $M_1=6.4$, $M_2=11.8$; (b) $M_1=5.04$, $M_2=9.08$; (c) $M_1=-3.5$, $M_2=-1.25$; (d) $M_1=-3.04$, $M_2=-7.08$; (e) $M_1=8.1$, $M_2=-6.1$; (f) $M_1=6.02$, $M_2=-4.02$

Fig. 10 Regular and symmetrical scanning trajectories when $|M_1|\neq|M_2|$. (a) $M_1=6.4$, $M_2=11.8$; (b) $M_1=5.04$, $M_2=9.08$; (c) $M_1=-3.5$, $M_2=-1.25$; (d) $M_1=-3.04$, $M_2=-7.08$; (e) $M_1=8.1$, $M_2=-6.1$; (f) $M_1=6.02$, $M_2=-4.02$

## 5 结 论

基于非近轴光线追迹算法对光楔扫描系统的正向问题进行求解,得到不同速度比下的花瓣形扫描轨迹。根据所得轨迹提出一种计算轨迹点数和花瓣数的简便方法,即轨迹点数等于$\left|360/\omega_1\right|$、$\left|360/\omega_2\right|$和$\left|360/\omega_3\right|$的

最小公倍数，花瓣数等于轨迹点与坐标原点的距离曲线的极小值点个数。在此基础上，根据速度比的绝对值、小数部分和小数位数对其进行分类，建立由速度比计算花瓣数的关系式，进而总结速度比与扫描轨迹之间的规律，并通过轨迹点数和花瓣数评估不同速度比对应扫描轨迹的扫描时间和覆盖率。

双光楔扫描轨迹有如下规律：$M$为正数时，扫描轨迹为内花瓣；$M$为负数时，扫描轨迹为外花瓣。$M$为整数时，不同速度比对应的扫描时间相同；$M$为小数时，若小数位数相同，则每一种类型的速度比对应的扫描时间分别相同，若小数位数不同，则小数位数越大，对应的扫描时间越长，因此速度比的小数位数不宜过多。对于每一种类型的速度比，当$M$同号时，$|M|$越大，则扫描轨迹覆盖率越大。此外，不同速度比可能有相同的花瓣数，$|M|<1$时的扫描轨迹也可转换成$|M|>1$时的扫描轨迹，这两种情况的扫描时间和覆盖率也可通过速度比对应的轨迹点数和花瓣数进行评估。三光楔扫描轨迹有如下规律：只有当速度比分别取$M_1$和$M_2$的双光楔的扫描轨迹花瓣数成倍数（1～2倍），其轨迹点数也成倍数（1～2倍）时，三光楔扫描轨迹才是规则、对称且不存在大片扫描盲区的花瓣形轨迹，其中：当$M_1$和$M_2$同正时，扫描轨迹为内花瓣；当$M_1$和$M_2$同负或异号时，扫描轨迹为外花瓣。三光楔扫描轨迹的扫描时间和扫描覆盖率可沿用双光楔扫描轨迹的规律进行评估。所得规律可在光楔扫描系统的实际应用中合理确定速度比，以选取满足扫描效率要求的扫描轨迹，光楔扫描轨迹对速度比的取值较为敏感，由于电机转速控制存在误差，实际速度比会与设定速度比存在一定偏差，后续可进一步探究此类偏差对扫描轨迹的影响。

## 参 考 文 献


[1] Kim B S, Gibson S, Tsao T C. Adaptive control of a tilt mirror for laser beam steering[C]//Proceedings of the 2004 American Control Conference, June 30-July 2, 2004, Boston, MA, USA. New York: IEEE Press, 2005: 3417-3421.

[2] 李焱, 曹立华, 王弟男. 惯导平台下舰载光电搜索跟踪系统的控制[J]. 光学 精密工程, 2011, 19(5): 1126-1133.
Li Y, Cao L H, Wang D N. Controlling of shipborne optoelectronic searching and tracking system based on inertial navigation platform[J]. Optics and Precision Engineering, 2011, 19(5): 1126-1133.

[3] Chen C B. Beam steering and pointing with counter-rotating grisms[J]. Proceedings of SPIE, 2007, 6714: 671409.

[4] Winsor R, Braunstein M. Conformal beam steering apparatus for simultaneous manipulation of optical and radio frequency signals[J]. Proceedings of SPIE, 2006, 6215: 62150G.

[5] Schwarze C. A new look at risley prisms[J]. Photonics Spectra, 2005, 40(6): 67-70.

[6] Philip J, Henry G, Vassili S. Wide-angle achromatic prism beam steering for infrared countermeasures and imaging applications: solving the singularity problem in the two-prism design[J]. Optical Engineering, 2007, 46(11): 113001.

[7] Li A H, Liu X S, Sun W S. Forward and inverse solutions for three-element Risley prism beam scanners[J]. Optics Express, 2017, 25(7): 7677-7688.

[8] 范大鹏, 周远, 鲁亚飞, 等. 旋转双棱镜光束指向控制技术综述[J]. 中国光学, 2013, 6(2): 136-150.
Fan D P, Zhou Y, Lu Y F, et al. Overview of beam steering technology based on rotational double prisms[J]. Chinese Optics, 2013, 6(2): 136-150.

[9] Schundler E, Carlson D, Vaillancourt R, et al. Compact, wide field DRS explosive detector[J]. Proceedings of SPIE, 2011, 8018: 80181O.

[10] 江伦, 胡源, 王超, 等. 一点对多点同时空间激光通信光学系统研究[J]. 光学学报, 2016, 36(5): 0506001.
Jiang L, Hu Y, Wang C, et al. Optical system in one-point to multi-point simultaneous space laser communications[J]. Acta Optica Sinica, 2016, 36(5): 0506001.

[11] Lu S W, Gao M, Yang Y, et al. Inter-satellite laser communication system based on double Risley prisms beam steering[J]. Applied Optics, 2019, 58(27): 7517-7522.

[12] 李福巍, 张运强, 潘国庆. 基于双光楔的双模光学系统设计分析[J]. 航空兵器, 2018, 25(1): 43-46.
Li F W, Zhang Y Q, Pan G Q. Design and analysis of dual-mode optical system based on dual-wedge[J]. Aero Weaponry, 2018, 25(1): 43-46.

[13] 朱精果, 李锋, 黄启泰, 等. 机载激光雷达双光楔扫描系统设计与实现[J]. 红外与激光工程, 2016, 45(5): 0502001.
Zhu J G, Li F, Huang Q T, et al. Design and realization of an airborne LiDAR dual-wedge scanning system[J]. Infrared and Laser Engineering, 2016, 45(5): 0502001.

[14] Marshall G F. Risley prism scan patterns[J]. Proceedings of SPIE, 1999, 3787: 74-86.

[15] Dimb A L, Duma V F. Symmetries of scan patterns of laser scanners with rotational risley prisms[J]. Symmetry, 2023, 15(2): 336.

[16] Clark C S, Gentile S. Flight miniature Risley prism mechanism [J]. Proceedings of SPIE, 2009, 7429: 74290G.

[17] Boisset G C, Robertson B, Hinton H S. Design and construction of an active alignment demonstrator for a free-space optical interconnect[J]. IEEE Photonics Technology Letters, 1995, 7(6): 676-678.

[18] Lavigne V, Ricard B. Fast Risley prisms camera steering system: calibration and image distortions correction through the use of a three-dimensional refraction model[J]. Optical Engineering, 2007, 46(4): 043201.

[19] Ostaszewski M, Harford S, Doughty N, et al. Risley prism beam pointer[J]. Proceedings of SPIE, 2006, 6304: 630406.

[20] Wolft W L, Zissis G J. Optical-mechanical scanning techniques and devices[D]. Michigan: Environmental Research Institute of Michigan, 1989.

[21] Jeon Y G. Generalization of the first-order formula for analysis of scan patterns of Risley prisms[J]. Optical Engineering, 2011, 50(11): 113002.

[22] Li Y J. Third-order theory of the Risley-prism-based beam steering system[J]. Applied Optics, 2011, 50(5): 679-686.

[23] Garcia-Torales G, Strojnik M, Paez G. Risley prisms to control wave-front tilt and displacement in a vectorial shearing interferometer[J]. Applied Optics, 2002, 41(7): 1380-1384.

[24] Sirohi R S, Kothiyal M P. Double wedge plate shearing interferometer for collimation test[J]. Applied Optics, 1987, 26(19): 4054-4056.

[25] Gibson J L, Duncan B D, Bos P, et al. Wide-angle beam steering for infrared countermeasures applications[[J]. Proceedings of SPIE, 2002, 4723: 100-111.

[26] Li Y J. Closed form analytical inverse solutions for Risley-prism-based beam steering systems in different configurations[J]. Applied Optics, 2011, 50(22): 4302-4309.

[27] 李晓彤, 岑兆丰. 几何光学·像差·光学设计[M]. 3版. 杭州: 浙

江大学出版社, 2014: 5-6.
Li X T, Cen Z F. Geometrical optics, aberrations and optical design[M]. 3rd ed. Hangzhou: Zhejiang University Press, 2014: 5-6.

# Selection Method of Risley Prisms Scanning Trajectory Based on Velocity Ratio

Duan Linsen[1], Xie Hongbo[1], Ma Jun[2*], Yang Lei[1]

[1]*Key Laboratory of Optoelectronics Information Technology, School of Precision Instrument and Optoelectronics Engineering, Tianjin University, Tianjin* 300072, *China*;

[2]*School of Armament Science and Technology, Xi'an Technological University, Xi'an* 710021, *Shaanxi*, *China*

## Abstract

**Objective** The Risley prism scanning system is a useful supplement to traditional rotating frame and mirror scanning systems. It features a compact structure, low optical loss, excellent dynamic performance, and a large scanning field of view, and has broad application prospects in lidars, laser communication, and laser guidance. In the practical applications of this system, it is important to select the scanning trajectory reasonably, which will directly affect the scanning efficiency of the system and the acquisition probability of the target. When the parameters and relative positions of the Risley prism are determined, the rotation velocity ratio of the Risley prism is variable and controllable to obtain the scanning trajectories of different shapes. We aim to study the relationship between the velocity ratio with the number of scanning points and petals, then summarize the internal rules of the velocity ratio and scanning trajectory, and evaluate the scanning time and coverage rate of the scanning trajectory under different velocity ratios. Therefore, our study has a guiding significance for selecting the scanning trajectory that meets the scanning efficiency requirements.

**Methods** Firstly, the forward problem of the Risley prism is solved by the non-axial ray tracing algorithm, and the scanning trajectories under different velocity ratios can be obtained. Secondly, the number of scanning points is calculated according to the rotation velocity of the Risley prism and sampling interval, and the number of scanning petals is calculated according to the number of minimum points of the distance curve between scanning points and coordinate origin. Then, the velocity ratio is classified according to its absolute value and fractional part, and the formula for calculating the number of scanning petals by the velocity ratio is established. The scanning trajectory rules of the 2-element Risley prism are analyzed, and the scanning time and coverage rate under different velocity ratios are evaluated. Finally, the scanning trajectory of the 3-element Risley prism is regarded as the superposition and cancellation of the scanning trajectory of the 2-element Risley prism, and the scanning time and coverage rate can be evaluated according to the scanning trajectory rules of the 2-element Risley prism. Additionally, the condition for the 3-element Risley prism to obtain a regular symmetry scanning trajectory without a large scanning blind zone is proposed by analyzing the velocity ratio.

**Results and Discussions** The scanning trajectory of 2-element Risley prism has the following rules (Table 1 and Fig. 4). When $M$ is positive, the scanning trajectory is inner petal, and the trajectory is outer petal under negative $M$. When $M$ is an integer, the scanning time under different velocity ratios is the same, and when $M$ is a decimal, the scanning time under each type of velocity ratio is the same if the number of decimal places is the same. Under the different numbers of decimal places, the larger number of decimal places leads to longer scanning time. Therefore, the number of decimal places should not be too large. For each type of velocity ratio, when $M$ is of the same sign, the larger $|M|$ brings a larger coverage rate. The scanning trajectory of 3-element Risley prism has the following rules (Table 4 and Fig. 10): only when the scanning petals of 2-element Risley prism are doubled (1–2 times) with the velocity ratio of $M_1$ and $M_2$, and the scanning points are also doubled (1–2 times), the scanning trajectory of 3-element Risley prism is regular symmetry and has no large scanning blind zone. When $M_1$ and $M_2$ are both positive, the scanning trajectory is inner petal. When $M_1$ and $M_2$ are both negative or different signs, the scanning trajectory is the outer petal. Additionally, the scanning time and coverage rate of the 3-element Risley prism can be evaluated according to the scanning trajectory rules of the 2-element Risley prism.

**Conclusions** As the scanning trajectory of the Risley prism determines the scanning efficiency of the system and the acquisition probability of the target, it is important to study the method of selecting the scanning trajectory by analyzing the velocity ratio. Based on the non-axial ray tracing algorithm, the forward problem of the Risley prism scanning system is

solved. Then the petal-shaped scanning trajectories under different velocity ratios are obtained, and the number of scanning points and scanning petals are calculated, which is then adopted to summarize the rules between the scanning trajectory and velocity ratio. The scanning time and coverage rate of the scanning trajectory under different velocity ratios are evaluated. Meanwhile, the condition for the 3-element Risley prism to obtain a regular symmetry scanning trajectory without a large scanning blind zone is proposed. The obtained rules and conclusions can be employed to reasonably determine the velocity ratio in the practical applications of the Risley prism scanning system to select the scanning trajectory that meets the scanning efficiency requirements. However, the scanning trajectory of the Risley prism is sensitive to the velocity ratio, and there will be deviations between the actual and set velocity ratios in the rotation control. Therefore, the influence of such deviations on the scanning trajectory can be further explored.

**Key words** optical design; Risley prism; non-axial ray tracing; petal-shaped scanning trajectory; velocity ratio